The ABC model of recombination reinterpreted: Impact on understanding carrier transport and efficiency droop in InGaN/GaN light emitting diodes

M. A. Hopkins, D. W. E. Allsopp, M. J. Kappers, R. A. Oliver, and C. J. Humphreys

---

Articles you may be interested in

Burying non-radiative defects in InGaN underlayer to increase InGaN/GaN quantum well efficiency
Applied Physics Letters **111**, 262101 (2017); 10.1063/1.5007616

Shockley-Read-Hall and Auger non-radiative recombination in GaN based LEDs: A size effect study
Applied Physics Letters **111**, 022104 (2017); 10.1063/1.4993741

Impact of carrier localization on recombination in InGaN quantum wells and the efficiency of nitride light-emitting diodes: Insights from theory and numerical simulations
Applied Physics Letters **111**, 113501 (2017); 10.1063/1.5002104

Impact of crystal orientation on the modulation bandwidth of InGaN/GaN light-emitting diodes
Applied Physics Letters **112**, 041104 (2018); 10.1063/1.5019730

BInGaN alloys nearly lattice-matched to GaN for high-power high-efficiency visible LEDs
Applied Physics Letters **111**, 211107 (2017); 10.1063/1.4997601

Photo-induced droop in blue to red light emitting InGaN/GaN single quantum wells structures
Journal of Applied Physics **122**, 063103 (2017); 10.1063/1.4997608

The ABC model of recombination reinterpreted: Impact on understanding carrier transport and efficiency droop in InGaN/GaN light emitting diodes

M. A. Hopkins,[1] D. W. E. Allsopp,[1,a)] M. J. Kappers,[2] R. A. Oliver,[2] and C. J. Humphreys[2]

[1]*Department of Electronic and Electrical Engineering, University of Bath, Bath, United Kingdom*
[2]*Department of Materials Science and Metallurgy, University of Cambridge, 27 Charles Babbage Road, Cambridge CB3 OFS, United Kingdom*

The efficiency of light emitting diodes (LEDs) remains a topic of great contemporary interest due to their potential to reduce the amount of energy consumed in lighting. The current consensus is that electrons and holes distribute themselves through the emissive region by a drift-diffusion process which results in a highly non-uniform distribution of the light emission and can reduce efficiency. In this paper, the measured variations in the external quantum efficiency of a range of InGaN/GaN LEDs with different numbers of quantum wells (QWs) are shown to compare closely with the predictions of a revised ABC model, in which it is assumed that the electrically injected electrons and holes are uniformly distributed through the multi-quantum well (MQW) region, or nearly so, and hence carrier recombination occurs equally in all the quantum wells. The implications of the reported results are that drift-diffusion plays a far lesser role in cross-well carrier transport than previously thought; that the dominant cause of efficiency droop is intrinsic to the quantum wells and that reductions in the density of non-radiative recombination centers in the MQW would enable the use of more QWs and thereby reduce Auger losses by spreading carriers more evenly across a wider emissive region. © 2017 Author(s). All article content, except where otherwise noted, is licensed under a Creative Commons Attribution (CC BY) license (http://creativecommons.org/licenses/by/4.0/). https://doi.org/10.1063/1.4986434

INTRODUCTION

InGaN/GaN light emitting diodes (LEDs) are fast becoming the component of choice for many lighting applications due to their compactness, color control, and energy efficiency.[1–3] Despite this success, there are still ongoing questions about the spread of charge carriers injected into the multi-quantum wells (MQWs) between radiative recombination processes and non-radiative recombination[4–6] and leakage currents.[7,8] This has led to continuing interest in the impact of parameters such as the thickness of the quantum wells (QWs),[9] their composition,[10] and optimum number[11–14] on the LED internal quantum efficiency (IQE), and in applying the ABC model of recombination to studies of efficiency droop in InGaN/GaN LEDs.[4,7,15,16]

The ABC model was originally developed as a simple parameterization of the rates of recombination by which excess populations of free carriers in semiconductors are restored to thermal equilibrium values.[17] In it, the rate of radiative recombination is given by Bnp, where n is the excess density of electrons and p is the excess density of holes, Shockley-Read-Hall (SRH) non-radiative recombination by An or Ap depending on whether electrons or holes are the minority carriers, and by a third order term, given by Cn^2p or Cnp^2, frequently ascribed to the Auger effect,[17] but its origin remains of topical debate.[18–22] A, B, and C represent the rate constants of these recombination processes, but attempts to extract physically meaningful values for these

coefficients from measurements of the light output power versus forward bias current characteristics of InGaN/GaN light emitting devices (LEDs) are frustrated by several factors.

First, carriers that bypass the multi-quantum well region (MQW) either by tunnelling via defects through or thermionic emission over the electron blocking layer (EBL) form a part of the total current injected into the emissive region, but do not contribute to recombination in the QWs.[4,15,19] Next, it is often not possible to describe SHR recombination with a single-valued rate constant, especially when the dominant traps have electric-field dependent capture cross-sections. It is also widely thought that the QWs do not contribute equally to emitted optical power due to the highly non-uniform electron and holes distributions in the MQW,[7,11] a view supported by device simulation based on carrier drift-diffusion being the dominant mechanism for cross-well transport.[7,9,10,13]

Recent theoretical work has considered the possible impact of carriers occupying the higher-lying energy states of QWs on cross-well transport.[24] These states tend to couple together across individual QWs, especially in c-plane oriented MQWs, in which the polarization and oppositely-directed depletion field make a major contribution to the band edge variation, to provide a means for rapidly spreading injected carriers across a MQW by thermally assisted tunneling. Monte Carlo simulations have shown that this mechanism can result in much more uniform distributions of electrons and holes through the MQW than achieved by drift-diffusion alone.[24] A similar superlattice effect for

a)Author to whom correspondence should be addressed: d.allsopp@bath.ac.uk

spreading carriers more uniformly through the MQW by reducing the QW barrier thickness had been considered earlier as a way of combating efficiency droop by suppressing the onset of third order non-radiative recombination processes.[25,26] Thus, if carrier transport via thermally assisted tunneling was operative in the MQW of InGaN/GaN LEDs, this would impact on the optimum number of QWs.

In this paper, we present a study of the efficiency of a series of InGaN/GaN LED samples in which the number of QWs, N, varied from 3 to 15. The measured trends in the current dependence of the external quantum efficiency (EQE) are then fitted to a revised ABC model based on the assumption that electrons and holes are distributed uniformly through the MQW. This leads to modified rate constants for non-radiative recombination which explicitly depend on N.

EXPERIMENTAL METHODS

A set of blue InGaN/GaN MQW LEDs, in which the number of quantum wells varied from 3 to 15, were grown by metal-organic vapor phase epitaxy (MOVPE) on c-plane sapphire substrates with a miscut of 0.25 ± 0.1 towards (11–20). The resulting epitaxy had a threading defect density of approximately $4 \times 10^8 \, \text{cm}^{-2}$. The MQW was grown using a two-temperature method, in which the growth temperature is ramped up over 90 s to 846 °C immediately after the InGaN growth, under ammonia but with no metal-organic fluxes, with the barrier growth beginning at 846 °C, increasing to 880 °C for most of the duration of the GaN barrier growth.[27] The structure of all the samples was as follows: 2.0 μm unintentionally doped GaN, 2.5 μm thick n-GaN with a Si doping concentration of $4 \times 10^{18} \, \text{cm}^{-3}$, 23 nm of Si-doped $In_{0.05}Ga_{0.95}N$ (same Si doping level as the preceding n-GaN), and $\sim$3 nm of unintentionally doped GaN. The MQWs consisted of either 3, 5, 7, 10, or 15 InGaN wells with an average thickness of 2.4 ± 0.3 nm sandwiched between GaN quantum barriers with an average thickness of 7.0 ± 0.4 nm, with an average indium content of $12 \pm 1\%$ and a peak emission wavelength between 445 and 452 nm. The QWs were then capped by a 12 nm wide $Al_{0.17}Ga_{0.83}N$:Mg electron blocking layer (EBL) and a 120 nm Mg doped p-GaN layer with a doping concentration of $3 \times 10^{19} \, \text{cm}^{-3}$.

The wafers were processed into lateral devices, 420 μm $\times$ 400 μm in size, with an inter-digitated electrode design to enhance the current uniformity. The areas of the mesa and the transparent p-contact were $1.48 \times 10^{-3} \, \text{cm}^2$ and $1.17 \times 10^{-3} \, \text{cm}^2$, respectively. The transparent p-contact consisted of evaporated Ni/Au (9/9 nm thick) annealed in oxygen at 500 °C for 5 min.

Artifacts associated with the device structure and measurement technique must be accounted for, if not eliminated, for reliable ABC modeling based on the curve fitting of the measured external quantum efficiency (EQE) characteristics. The non-uniform current flow in a LED distorts its EQE versus injected carrier density characteristic and has been cited as a cause of the efficiency droop.[8,28,29] In the devices fabricated, the sheet resistance of the n-GaN was 14.5 $\Omega/\square$ and that of the combined p-GaN layer and transparent p-contact was 25–30 $\Omega/\square$. The impact of this imbalance was measured
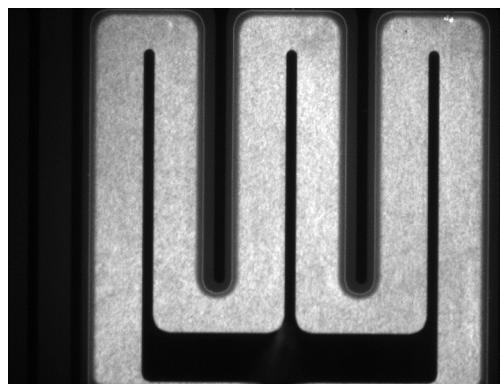

FIG. 1. Photograph of a device from wafers with 3 QWs at 100 mA (worst case).

by taking CCD camera images of the finished devices, such as the one shown in Fig. 1. From these, it was found that the electroluminescence (EL) varied by at most 10% across a chip over a wide range of currents. The extent to which the efficiency versus current graphs were distorted by such current non-uniformity was investigated by reducing the sheet resistance of the transparent p-contact to closely match that of the n-GaN by depositing another thin layer of Ni over the annealed Ni/Au contacts to produce LEDs with the optimum equal access resistances for uniform current spreading.[30]

The electrical and light output characteristics of the LEDs were measured on the wafer as a function of current up to a maximum of 0.75 A, equivalent to a current density of 650 A/cm². For drive currents up to 0.5 A, the light output was measured from the top (p-side) of the device with an integrating sphere (Newport) placed $\sim$5 mm above to enable low-profile probes to connect devices to a pulsed current source (Keithley 2600B) which applied 0.5 ms duration pulses on a low duty cycle. For drive currents of 0.5–0.75 A, 10 μs duration pulses were applied from a high-speed source-measure unit (Keithley 2520) to reduce yet further any Joule heating. In this system, the light output was measured from the substrate side with a large area ($\sim 1 \times 1 \, \text{cm}^2$) calibrated Si photodiode placed directly below a glass sample stage. In all measurements, a fixed time interval of 500 ms between pulses was used.

Figure 2 presents the normalized EQE versus forward current graphs measured before and after depositing the additional Ni layer for devices to show the worst case (5 QWs) and typical cases (3 and 7 QWs) of the effect on the light output-current characteristics of improving the current spreading by adding the extra Ni layer to the p-contacts. The changes in the efficiency curves shown in Fig. 2 were found to have very little impact on ABC curve fitting. From this, we conclude that non-uniform current spreading had little influence on the efficiency droop observed in our LEDs.

The spectral output of each device was measured so that the results could be corrected for $\sim$7 nm variation in the peak emission wavelength from sample to sample and for its blue-shift with increasing drive currents. The correction is required because the wavelength dependence of the photodetector responsivity can cause the LED efficiency droop to appear greater than it really is. Detailed mapping of the
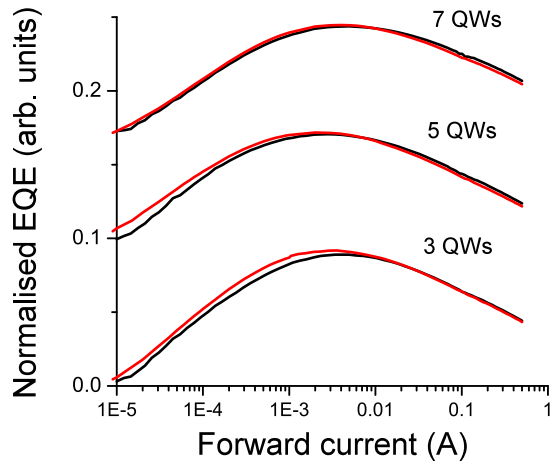
FIG. 2. Normalized EQE as a function of the forward current from the same devices before (black) and after (red) reducing the p-contact resistance by the deposition of extra Ni for a device with 3, 5, and 7 QWs. The normalized EQE curves have been offset from each other for visual clarity and the forward current is plotted on a logarithmic scale.

current-voltage characteristics ensured that only devices with very low ohmic leakage currents were considered, so that the ABC analysis excluded devices with efficiency curves distorted by parasitic currents.[4] The resulting light output-current plots underestimate, but are proportional to, the true EQE-current characteristics and, as such, are hereafter referred to as the EQE curves.

RESULTS

The EQE (η) of devices measured from the top and bottom faces of the devices are plotted as a function of the device current density in Figs. 3(a) and 3(b), respectively. (Here, the EQE is defined as the photodetector current, I_p, divided by the LED forward bias current, I_f.) There was some variation between devices and so representative results from each wafer are shown in Figs. 3(a) and 3(b). The color scheme used for displaying the results is "spectrally ordered" such that the red curves correspond to 3 QW LEDs, yellow 5 QW LEDs through to violet curves for the 15 QW LEDs.

There was a small difference in the absolute value in the η when measured from the bottom of a device rather than the top. This difference became larger in the devices in which the current spreading was improved by adding the thin Ni layer to the p-GaN due to the increased reflectivity of the top surface. Based on this observation, any differences between the top and bottom face measurements of the light extraction efficiency are due to differences in the optical impedance between the MQW and the upper and lower surfaces of the LEDs. For example, the bottom face measurements were less effected by the reflectivity of the p-contact and so these results formed the basis of the analysis below; although using the top face measurements instead produced little difference in the curve fitting parameters.

From Figs. 3(a) and 3(b), it can be seen that the efficiency droop decreased with the increasing number of QWs, so that at higher current densities, the devices with 10 and 15 QWs were the most efficient. A similar trend with a number of QWs was observed by Zhang *et al.*[14]
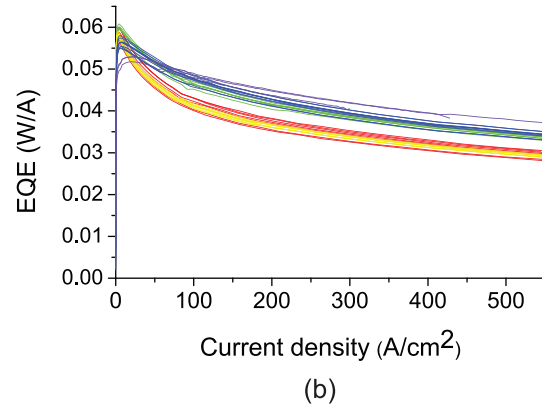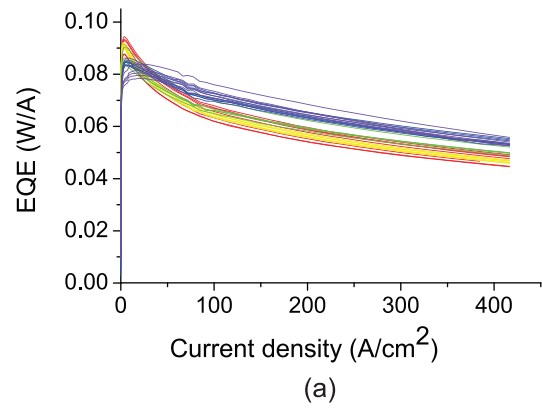

FIG. 3. EQE vs current density plots of devices with 3 (red), 5 (yellow), 7 (green), 10 (blue), and 15 (violet) QWs measured from (a) the top and (b) the bottom of the device.

Finally, the efficiency droop on the same device was greater in the measurements made from the top due to device heating caused by the use of longer 0.5 ms pulses rather than the 10 μs wide pulses used when measuring η from the substrate side of the LEDs. From the above tests of our experimental methods, we found that contributions to the shape of the efficiency versus drive current curves from current crowding, the wavelength dependence of the photodetector responsivity and Joule heating was negligibly small for applied forward currents up to currents densities of 650 A/cm^2.

The results presented in Fig. 3(b) were analyzed using the revised ABC model described in the Revised ABC Model Section.

REVISED ABC MODEL

The form of the ABC model devised by Dai *et al.*[31] provides a convenient starting point as it takes into account otherwise problematic tunnelling and overflow currents[15,16] by expressing these as a power series in n, the average electron density in the MQW. Justification for this approximation comes from the observation that tunneling and overflow currents in InGaN/GaN LEDs can be accounted for empirically by using a diode equation with a larger ideality factor to describe their current-voltage characteristics.[32,33] Using this model with the assumption that the carriers are evenly distributed over N wells, with an electron density of n and a hole density of $p = sn$ (s a bias independent constant) in each QW the total current, I_f, can be expressed as[31]
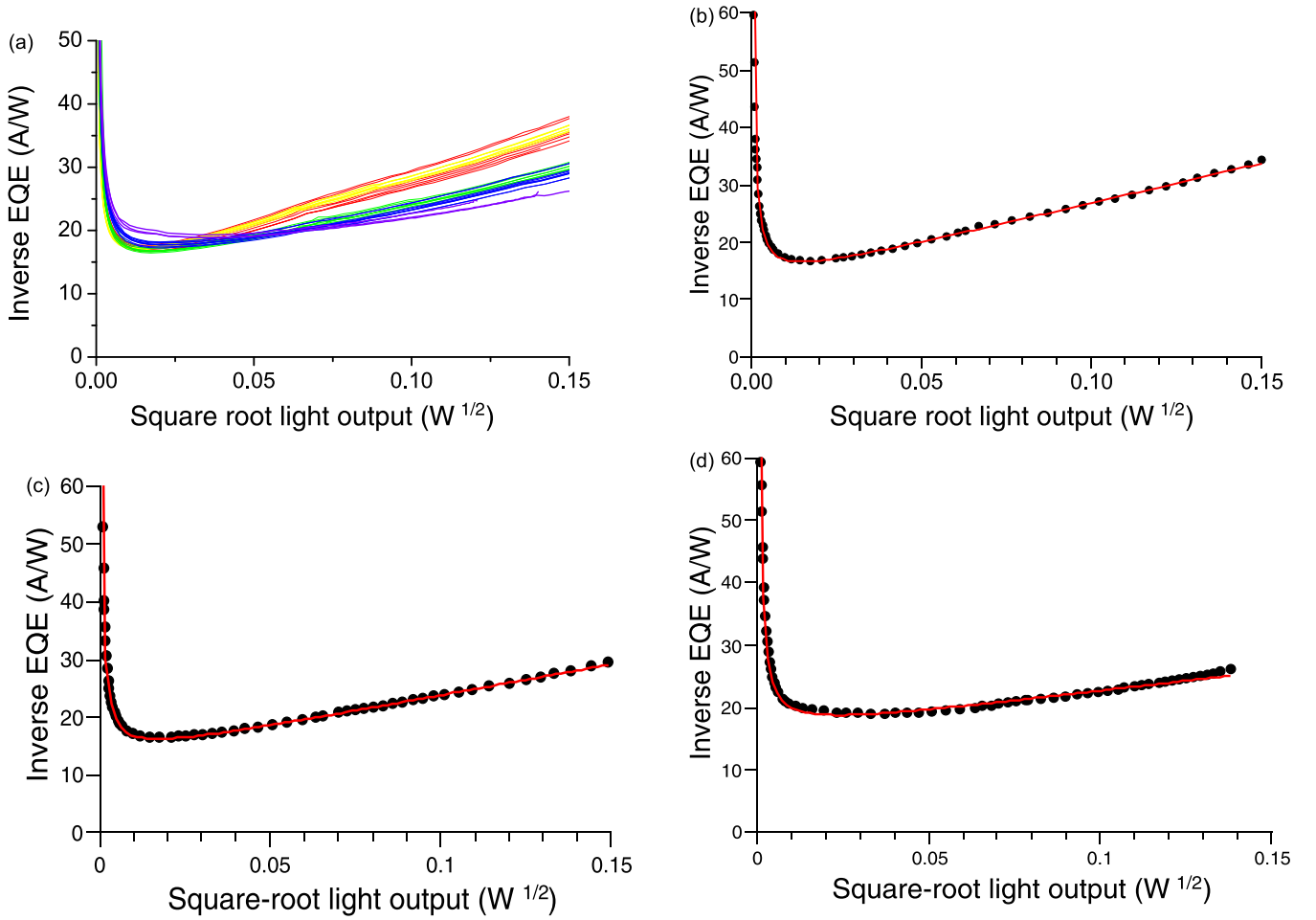
FIG. 4. (a) Reciprocal of EQE vs square-root of the light output of devices with 3, 5, 7, 10, and 15 QWs measured from the bottom of the device. (b)–(d) $\alpha\beta\gamma$ fits to η^{-1} versus square root of the light output of the LEDs with 3, 7, and 15 QWs.

$$I_f = qvsN \left[A'n + B'n^2 + C'n^3 + O'(n^m) \right]. \quad (1)$$

In Eq. (1), $A' = A + a$; $B' = B + b$; $C' = C + c$, where A, B, and C are the recombination rate constants, and a, b, and c account for the contributions to the power series from the tunneling and overflow currents. The terms a, b, and c also take into account any carrier dependence (equivalently electric field dependence) of A, B, and C. $O'(n^m)$, where m is an integer > 3, represents higher order terms in n, while q, v, and N are, respectively, the unit of charge, the effective recombination volume of one period of the MQW, and the number of wells. The concept of effective recombination volume is introduced to account for the possibility that carriers confined to the QWs may tunnel to nearby defects in the quantum barriers adjacent to the InGaN layers from where they can recombine non-radiatively,[34,35] or even radiatively.[36]

With the assumption that the injected electrons and holes are uniformly distributed across the MQW it follows, that each QW contributes equally to the light output power (P_l), so that in a measurement of LED efficiency, the photocurrent, I_p, will be given by

$$I_p = k\eta_{ex} vsNBn^2, \quad (2)$$

where k is a constant that takes into account power-to-current conversion and that the measurement system does not detect all the extracted optical power and η_{ex} is the light extraction efficiency. Using Eqs. (1) and (2), the external quantum efficiency becomes, on neglect of terms of order n^4 and higher

$$\frac{1}{\eta} = \frac{I_f}{I_p} = \alpha \frac{1}{I_p^{1/2}} + \beta + \gamma I_p^{1/2}, \quad (3)$$

where new curve fitting parameters α, β, and γ are given by

$$\alpha = \sqrt{\frac{vs}{k\eta_{ex}}} \frac{q(A+a)}{B^{1/2}} N^{1/2}, \quad (4a)$$

$$\beta = \frac{q}{k\eta_{ex}} (1 + b/B), \quad (4b)$$

$$\gamma = \frac{q}{(k\eta_{ex})^{3/2} \sqrt{vs}} \frac{(C+c)}{B^{3/2}} \frac{1}{N^{1/2}}. \quad (4c)$$

Equation (3) reproduces the dependence of EQE on the photon emission rate derived by Binder *et al.*[37] However, the outcome of revisiting the ABC model under the assumption that injected electrons and holes spread uniformly across the MQW is that effective rate coefficients α and γ now depend on $N^{1/2}$ and $N^{-1/2}$, respectively.
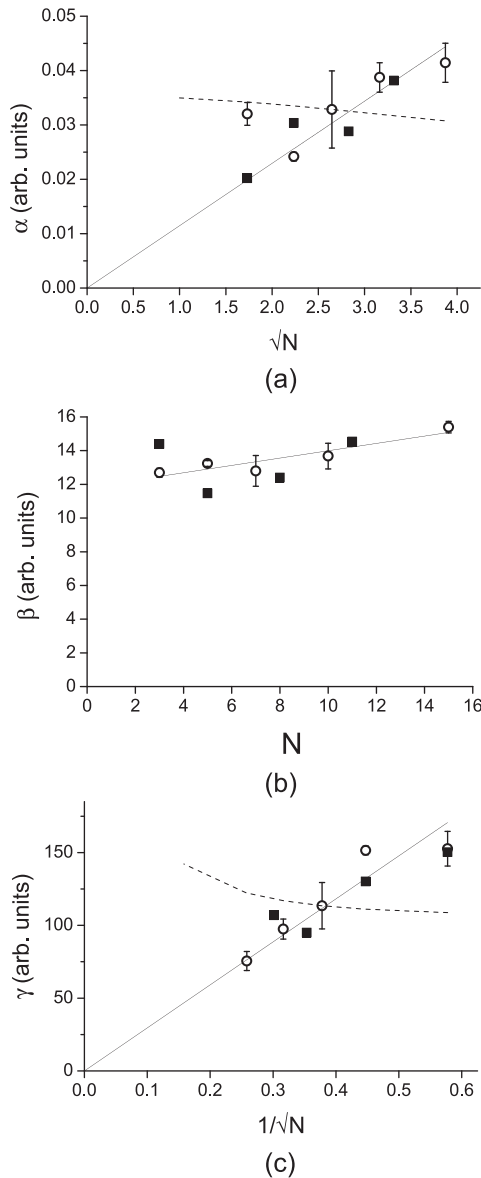
FIG. 5. (a) α versus $\sqrt{N}$, (b) β versus N, and (c) γ versus $1/\sqrt{N}$. The open circle data points are for the α, β, and γ values obtained from the fits to the EQE measurements reported here. The black lines are a straight line fits to these results. In the case of α and γ data, these trend lines are forced through the origin, with the $N = 3$ point excluded for the fitting to the α results. The error bars correspond to the standard deviation in each datum obtained from applying the αβγ fitting to typically 10 or more devices of each type. The closed square symbols are from the αβγ fitting of the data of Zhang *et al.*[14] and were excluded from trend line fitting. The dashed lines in (a) and (c) show the trends in α and γ if exponentially decaying distributions of electrons and holes occur in the MQW (see text).

To enable comparison between measurement and the formulae in Eqs. (3) and (4), the curve fitting tool in Origin (OriginLab) was used to analyze the graphs of η^{-1} versus $\sqrt{I_p}$ curves. Figure 4(a) shows the data plotted in Fig. 3(b) re-plotted as η^{-1} versus $\sqrt{I_p}$, while Figs. 4(b)–4(d) show typical fits of the measured data for 3, 7, and 15 QW LEDs, to a 3rd order polynomial of the form of Eq. (3). Such fits were characteristic of all the low leakage devices tested. In their work, Dai *et al.*[31] had to include higher terms in *n* to obtain a satisfactory fit to their EQE versus drive current characteristics. We found that, after correcting the results for the apparent efficiency reduction due to the lowering of the

photodetector responsivity with the blue-wavelength shift of the light emission with increasing current and rigorously minimizing the effect of Joule heating, the efficiency curves were a good fit to the 3rd order αβγ model up to a current density of $650 \, \text{A/cm}^2$ in all cases. The least good fits were obtained from the devices with 15 QWs [Fig. 4(d) demonstrates the worst case], but even then the difference between the 3rd or 4th order polynomial fits was small. From these observations, we concluded that the 3rd order αβγ model was the most appropriate for describing the trends in the data.

Figures 5(a)–5(c) show the variation in α with $N^{1/2}$, β with N, and γ with $N^{-1/2}$ (open circles in each graph), where α, β, and γ were obtained from fitting the results in Fig. 4(a) and Eq. (3). The device processing and measurements were repeated on other quarter-wafer fragments processed at different times and with p-contacts fabricated in differing ways. Despite a small change in η_{ex}, these samples showed the same trends seen in Fig. 5. The lines in Figs. 5(a) and 5(c) are best fit trend lines forced through the origin to test compliance with Eqs. (4a) and Eq. (4c), i.e., when the case when injected electrons and holes are uniformly distributed across the MQW.

DISCUSSION

There are several striking features in Fig. 5. First, there is a marked decrease, by a factor of 2.6, in γ with an increasing number of QWs with the trend closely following the $N^{-1/2}$ dependence predicted in Eq. (4c) [solid line in Fig. 5(c)]. Next, coefficient α increases by a factor of about 1.6 with the increasing number of QWs, with the trend in the data following the $N^{1/2}$ dependence given by Eq. (4a) [solid line in Fig. 5(a)], but with more scatter than the fit of γ to its predicted $N^{-1/2}$ dependence. β also increased linearly with N, but by just ∼20% as N increases from 3 to 15.

While the trends in Figs. 5(a) and 5(c) are well described by the assumption that carrier re-combination occurs uniformly across all the QWs, other possible causes of such behavior need to be considered, especially since β also increased, albeit slowly, with N. This behavior is not predicted by Eq. (4b), implying the possibility that other parameter variations could have contributed to the trends shown in Figs. 5(a) and 5(c). In particular, the roles of terms *a*, *b*, and *c*, included in Eqs. (4a)–(4c) to account for any leakage current must be considered.

It is implicit in the derivation of the $N^{\pm 1/2}$ dependences of α and γ that each QW also contributes equally to electron leakage, if significant. This can only occur if two conditions are met. First, transporting electrons to the QWs nearest to the EBL (i.e., those from which tunneling and thermionic emission through or over the EBL is most likely) is not the rate limiting process in determining their distribution through the MQW. Second, the electron and hole distributions through the MQW are uniform, or nearly so, a condition that follows from the first. Detailed simulations of carrier distributions and electron leakage currents reveal that drift-diffusion acting alone will not give rise to uniform electron and holes distributions in an InGaN/GaN LED,[6,7,10] and

therefore, would not result in the $N^{\pm 1/2}$ dependence of α and γ seen in Figs. 5(a) and 5(c).

Further, any increase in the electron leakage current with an increasing number of QWs would be represented by increases in the values of a, b, and c in Eq. (1) to cause increases in α, β, and γ with N. Again, this is contrary to observation with the implication that a, b, and c are all much smaller than coefficients A, B, and C, and hence, systematic changes in the electron leakage with N are not the cause of the trends seen in Figs. 5(a) and 5(c). The small increase in β with N supports this interpretation.

According to Eq. (4c), other parameter changes that could cause the observed decrease in γ with the increasing number of QWs include systematic increases in η_{ex} or B. However, such changes would also cause both α and β to decrease with N, contrary to the evidence in Figs. 5(a) and 5(b). Therefore, it is unlikely that changes in η_{ex} or B are the cause of the systematic variations in α and β with $N^{\pm 1/2}$ seen in Figs. 5(a) and 5(c).

We conclude that the revised ABC model, based on the assumption that electrically injected electrons and holes are uniformly distributed through the MQW or nearly so, accurately describes the trends of α and γ with the increasing QW number seen in Figs. 5(a) and 5(b). Since carrier transport by drift-diffusion acting alone is unlikely to produce such an outcome, the possibility of cross-well transport mechanisms in c-plane oriented InGaN/GaN MQWs acting in parallel now have to be considered.

Of the mechanisms that can release carriers with a thermalized energy distribution from the QWs, Poole-Frenkel emission and defect-assisted tunneling from the low energy confined particle states of the QWs will give rise to characteristic, electric field dependent current-voltage (I-V) dependences.[38] However, the I-V characteristics of the LEDs reported here complied with the behavior reported by Binder *et al.*,[37] namely, that of a pn junction diode in which the forward bias fluxes of electrons and holes feed both radiative and non-radiative recombination in the junction region (i.e., MQW) but modified by the presence of series and parallel resistances. Although in the devices used in the $\alpha\beta\gamma$ analysis, the leakage current was low, hence the parallel resistance was very large. This leaves tunneling via superlattice-like states as a mechanism by which carriers can rapidly spread across the MQW.

Superlattice states can exist in the energy range, where the sequential changes in the polarization with III-Nitride composition in a c-plane oriented InGaN/GaN MQW give rise to triangular-shaped quantum barriers between neighboring QWs. When the barriers are sufficiently thin, the quantum states of both carrier types couple together to form bands of superlattice states[24,26] to provide a route for carriers to tunnel rapidly across the MQW and form more widely spread electron and hole distributions.[26] Even with wider barriers, the difference in the steady state hole density across a 5-well MQW is predicted by Monte Carlo simulation to be just a factor of ~10 with the starting condition of a thermal equilibrium distribution of holes in the ladder of quantized states of the first QW and the rest empty.[24] Further, it was found that the transfer of both electrons and holes across the modelled 5 well MQW occurs on a sub-ps timescale.[24]

In a forward biased LED, both electrons and holes injected into the MQW will initially occupy these higher lying coupled subbands, rather than having the initial thermalized energy distribution assumed in Hammersley *et al.* Such direct carrier injection into the superlattice-like states of the quasi-sawtooth band profile is likely to promote still further rapid transport of both electrons and holes to yield more nearly uniform steady state distributions across the MQW.

As such, drift-diffusion would play a lesser role in cross-well carrier transport, even when enhanced by thermal re-emission of carriers from the QWs to above the barrier edge.[39,40] This conflicts with the conventional understanding of InGaN/GaN LED device physics, so we have tested our data by applying the above analysis to data extracted by digitizing Zhang *et al.* measurements of EQE curves for LEDs structures with 3, 5, 8, and 11 QWs (Fig. 4 of their paper).[14] The results are shown by the solid squares in Figs. 5(a) and 5(c). The fits of Zhang *et al.* data to the $N^{\pm 1/2}$ dependences and the overlap with the values of α and γ extracted from our own EQE measurements are remarkable, and demonstrate that these trends are not just an artifact of our samples and measurements. Rather, this re-working of their data supports the contention that electrically injected electrons and holes are more uniformly distributed through the MQW.

Since such carrier distributions conflict with the current understanding, there is arguably a need to identify the equivalent trends in the A and C coefficients with N, if drift-diffusion dominates cross-well transport. An analytic expression for the IQE variation with N can be derived if, within the MQW, the distributions of holes and electrons vary as $p_{i+1} = p_i \exp(-L/L_p)$ or $n_{i+1} = n_i \exp(L/L_n)$ ($i = 1$ to N) relative to their concentrations p_i and n_i in the neighboring QW nearer to the EBL, where L is the MQW period and L_p and L_n are characteristic decay lengths. Such distributions of electrons and holes reasonably approximate the predictions of LED models in which cross-well transport by drift-diffusion is assumed. If the injected current primarily feeds recombination in the MQW and if the radiative and non-radiative rate constants in every QW are the same as those in the QW nearest, the EBL vary only slowly [Fig. 5(b) shows this is reasonable in the case of β, i.e., B], then the total injected current is given by

$$I \approx A_1 \sum_{i=1}^{N} p_i + B_1 \sum_{i=1}^{N} p_i^2 + C_1 \sum_{i=1}^{N} p_i^3. \tag{5}$$

In Eq. (5), A_1, B_1, and C_1 are the rate constant values for the QWs nearest to the EBL. Dividing by the radiative recombination term in Eq. (5) yields the internal quantum efficiency

$$\frac{1}{\eta_{IQE}} \approx \alpha_1' \left[\frac{(1 - e^{-NL/L_p})(1 - e^{-L/L_p} e^{L/L_n})}{(1 - e^{-L/L_p})(1 - e^{-NL/L_p} e^{NL/L_n})} \right] + 1$$
$$+ \gamma_1' \left[\frac{(1 - e^{-NL/L_p} e^{2NL/L_n})(1 - e^{-L/L_p} e^{L/L_n})}{(1 - e^{-L/L_p} e^{2L/L_n})(1 - e^{-NL/L_p} e^{NL/L_n})} \right]. \tag{6}$$

The dashed lines in Figs. 5(a) and (5b), respectively, show the variation in the ratios α'_N/α'_1 and γ'_N/γ'_1 predicted in Eq. (6), but plotted as $N^{1/2}$ or $N^{-1/2}$ and renormalized so that the calculated values coincide with the respective $N = 7$ points in our measured data sets. The trend lines were obtained assuming $L_p = 100\,\text{nm}$ and $L_n = 400\,\text{nm}$ in Eq. (6), i.e., values that closely correspond to the electron and hole diffusion lengths in bulk GaN.[41] Clearly, the variations in α'_N/α'_1 and γ'_N/γ'_1 with N predicted by Eq. (6) are contrary to the $N^{\pm 1/2}$ trends shown by their equivalent values obtained from the measured efficiency curves, both our own and those of Zhang *et al.*[14]

However, the use of bulk values of the diffusion lengths of electrons and holes for cross-well transport in a MQW is open to question, because the thermal energy needed to re-release carriers trapped in the QWs will effectively reduce their mobility. Using values of $L_p = 20\,\text{nm}$ and $L_n = 50\,\text{nm}$, arbitrarily chosen to reflect the reduced carrier diffusion lengths in an MQW, instead also produced trends in α'_N/α'_1 with $N^{1/2}$ and γ'_N/γ'_1 with $N^{-1/2}$ with negative gradients. A similar outcome resulted when L_p and L_n were increased to 500 and 2000 nm, respectively.

From this exercise, it is concluded that carrier distributions similar to those expected if drift-diffusion was the main mechanism of cross-well transport, do not provide a basis for explaining the observed $N^{\pm 1/2}$ trends in the modified SRH and Auger recombination rate constants with a number of wells in the MQW. Further, the α and γ parameters extracted from the IQE curves obtained by Xia *et al.*[13] from their drift-diffusion simulations of LEDs with 3, 6, 9, 12, 15, and 18 QWs did not follow the respective $N^{\pm 1/2}$ trends shown in Figs. 5(a) and 5(c). These results are significant because the procedure applied to obtain α, β, and γ values was exactly the same as that used in analyzing the measured data, i.e., it did not rely on making additional assumptions as the derivation of Eq. (6) does.

It is worth noting that Laubsch *et al.* also obtained a best fit between IQE versus current density curves measured by electroluminescence and modelled IQE when uniform distributions of electrons and holes across the MQW are assumed in a rate equation model comprising defect-related SRH and Auger-like recombination as non-radiative loss and bimolecular radiative recombination mechanisms.[42] In another study of the effect of increasing the number of QWs from 5 to 7 in 380-nm UV-LEDs, Choi *et al.* found that the systematic changes they observed in the optical and electrical characteristics were best described by assuming uniform distributions of electrons and holes across the MQW.[43]

The conclusion that nearly uniform distributions of electrons and holes occur across the MQW, does not necessarily conflict with experiments in which a QW emitting at a longer wavelength has been used to identify the location in a MQW from which light is predominantly emitted.[23] The presence of a deeper or wider QW in a superlattice or MQW will both introduce electron and hole states localized to the different wells and disrupt the formation of the quasi-extended states by which free carriers would otherwise spread through the MQW by thermally-assisted tunneling.[24]

The fits of the extracted values of α and γ in Figs. 5(a) and 5(c) to their respective $N^{1/2}$ and $N^{-1/2}$ dependences predicted by the revised ABC model are also consistent with the assumptions that each QW in a MQW makes more or less the same contribution to all forms of carrier recombination and that carrier leakage currents are small, at least up to the current densities considered here. As such, it can be deduced that the recombination process or processes responsible for the efficiency droop are intrinsic to the MQW, even to a single QW.

Three mechanisms intrinsic to a MQW have been proposed for the cause of droop: Auger recombination,[20–22,44–46] carrier density activated defect recombination (DADR),[47,48] and tunneling-assisted non-radiative recombination,[35,36] the latter including trap-mediated Auger effects.[37] However, it is not possible from the results presented here to distinguish which such intrinsic mechanism is the primary cause for the efficiency droop in GaN-based LEDs.

CONCLUSIONS

In summary, we have measured the efficiency as a function of device current in a series of 5 InGaN LEDs, in which the number of QWs varied from 3 to 15. The efficiency droop was found to decrease with increasing number of QWs, and it was shown that this result cannot be explained by changes in the current uniformity or light extraction efficiency. The measured EQE curves were fitted to a revised ABC model, in which it was assumed that injected electrons and holes are uniformly distributed through the MQW so that carrier recombination occurred equally in all the QWs. The first and third order fitting coefficients, α and γ, obtained from our measurements, complied with $N^{1/2}$ and $N^{-1/2}$ dependences predicted by the new ABC model, with the fit of the revised C parameter (γ) to the predicted $N^{-1/2}$ dependence being particularly good.

Mechanisms which could have caused these effects were discussed and it was shown on phenomenological grounds that an electron leakage current was unlikely to have contributed significantly to the trends in the data and hence to the efficiency droop. The good agreement between the results and the revised ABC model carries the implication that drift-diffusion is not the dominant mechanism of cross-well transport in InGaN/GaN MQWs lying in the c-plane. Thermally-assisted tunneling of carriers occupying higher energy superlattice-like states and quantum states that couple together the QWs could act in parallel to explain the observed behavior. This contribution of thermally-assisted tunneling to cross-well transport could well be smaller in non-polar and semi-polar LEDs in which the quasi-sawtooth shaping of the potential profile in the MQW induced by the periodic polarization switching in c-plane InGaN/GaN LEDs is weaker or even absent, as in the case for QWs grown on the $(20\overline{2}\overline{1})$ plane.[49]

ACKNOWLEDGMENTS

The dataset on which this article is based can be found at https://researchdata.bath.ac.uk/id/eprint/377.

[1]E. F. Schubert, J. K. Kim, H. Luo, and J.-Q. Xi, Rep. Prog. Phys. **69**, 3069 (2006).

[2]M. R. Krames, O. B. Shchekin, R. Mueller-Mach, G. O. Mueller, L. Zhou, G. Harbers, and M. G. Craford, J. Disp. Technol. **3**, 160 (2007).

[3]M. H. Crawford, IEEE J. Sel. Top. Quantum Electron. **15**, 1028 (2009).

[4]J. Piprek, "Efficiency droop in nitride-based light-emitting diodes," Phys. Status Solidi A **207**, 2217 (2010).

[5]G. Verzellesi, D. Saguatti, M. Meneghini, F. Bertazza, M. Goano, G. Meneghesso, and E. Zanoni, J. Appl. Phys. **114**, 071101 (2013).

[6]J. Piprek, Appl. Phys. Lett. **107**, 031101 (2015).

[7]J. Piprek and Z. M. S. Li, Appl. Phys. Lett. **102**, 131103 (2013).

[8]G. B. Lin, E. F. Schubert, J. Cho, J. H. Park, and J. K. Kim, ACS Photon. **2**, 1013 (2015).

[9]Y.-L. Li, Y.-R. Huang, and Y.-H. Lai, J. Sel. Top. Quantum Electron. **15**, 1128 (2009).

[10]C. H. Wang, S. P. Chang, W. T. Chang, J. C. Li, Y. S. Lu, Z. Y. Li, H. C. Yang, H. C. Kuo, T. C. Lu, and S. C. Wang, Appl. Phys. Lett. **97**, 181101 (2010).

[11]A. David, M. J. Grundmann, J. F. Kaeding, N. F. Gardner, T. G. Mihopoulos, and M. R. Krames, Appl. Phys. Lett. **92**, 053502 (2008).

[12]S. Tanaka, Y. Zhao, I. Koslow, C.-C. Pan, H.-T. Chen, J. Sonoda, S. P. DenBaars, and S. Nakamura, Electron. Lett. **47**, 335–336 (2011).

[13]C. S. Xia, Z. M. Simon Li, Z. Q. Li, Y. Sheng, Z. H. Zhang, W. Lu, and L. W. Cheng, Appl. Phys. Lett. **100**, 263504 (2012).

[14]Y. P. Zhang, Z. H. Zhang, W. Liu, S. T. Tan, Z. G. Ju, X. L. Zhang, Y. Ji, L. C. Wang, Z. Kyaw, N. Hasanov, B. B. Zhu, S. P. Lu, X. W. Sun, and H. V. Demir, Opt. Express **23**, A34–A42 (2015).

[15]S. Karpov, Opt. Quantum Electron. **47**, 1293 (2015).

[16]J. Piprek, F. Römer, and B. Witzigmann, Appl. Phys. Lett. **106**, 101101 (2015).

[17]N. F. Mott, Solid State Electron. **21**, 1275 (1978).

[18]L. Wang, Z.-H. Zhang, and N. Wang, IEEE J. Quantum Electron. **51**, 3200109 (2015).

[19]G. B. Lin, D. Meyaard, J. Cho, E. F. Schubert, H. Shim, and C. Sone, Appl. Phys. Lett. **100**, 161106 (2012).

[20]K. W. Williams, N. R. Monahan, D. D. Koleske, M. H. Crawford, and X.-Y. Zhu, Appl. Phys. Lett. **108**, 141105 (2016).

[21]F. Nippert, S. Y. Karpov, G. Callsen, B. Galler, T. Kure, C. Nenstiel, M. R. Wagner, M. Strassburg, H. J. Lugauer, and A. Hoffmann, Appl. Phys. Lett. **109**, 161103 (2016).

[22]A. Nirschl, M. Binder, M. Schmid, I. Pietzonka, H.-J. Lugauer, R. Zeisel, M. Sabathil, D. Bougeard, and B. Galler, Opt. Express **24**, 2971 (2016).

[23]B. Galler, A. Laubsch, A. Wojcik, H. Lugauer, A. Gomez-Iglesias, M. Sabathil, and B. Hahn, Phys. Status Solidi C **8**, 2372 (2011).

[24]S. Hammersley, M. J. Davies, P. Dawson, R. A. Oliver, M. J. Kappers, and C. J. Humphreys, Phys. Status Solidi B **252**, 890 (2015).

[25]D. A. Zakheim, A. S. Pavluchenko, and D. A. Bauman, Phys. Status Solidi C **8**, 2340 (2011).

[26]D. A. Zakheim, A. S. Pavluchenko, D. A. Bauman, K. A. Bulashevich, O. V. Khokhlev, and S. Y. Karpov, Phys. Status Solidi A **209**, 456 (2012).

[27]R. A. Oliver, F. C.-P. Massabuau, M. J. Kappers, W. A. Phillips, E. J. Thrush, C. C. Tartan, W. E. Blenkhorn, T. J. Badcock, P. Dawson, M. A. Hopkins, D. W. E. Allsopp, and C. J. Humphreys, Appl. Phys. Lett. **103**, 141114 (2013).

[28]H.-Y. Ryu and J. I. Shim, Opt. Express **19**, 2886 (2011).

[29]C.-K. Li and Y.-R. Wu, IEEE Trans. Electron. Devices **59**, 400 (2012).

[30]E. F. Schubert, *Light-Emitting Diodes*, 2nd ed. (Cambridge University Press, New York, 2006).

[31]Q. Dai, Q. Shan, J. Wang, S. Chhajed, J. Cho, E. F. Schubert, M. H. Crawford, D. D. Koleske, M.-H. Kim, and Y. Park, Appl. Phys. Lett. **97**, 133507 (2010).

[32]J. M. Shah, Y.-L. Li, T. Gessmann, and E. F. Schubert, J. Appl. Phys. **94**, 2627 (2003).

[33]D. Zhu, J. Xu, A. N. Noemaun, J. K. Kim, E. F. Schubert, M. H. Crawford, and D. D. Koleske, Appl. Phys. Lett. **94**, 081113 (2009).

[34]N. I. Bochkareva, V. V. Voronenkov, R. I. Gorbunov, A. S. Zubrilov, Y. S. Lelikov, P. E. Latyshev, Y. T. Rebane, A. I. Tsyuk, and Y. G. Shreter, Appl. Phys. Lett. **96**, 133502 (2010).

[35]N. I. Bochkareva, Y. T. Rebane, and Y. G. Shreter, Semiconductors **49**, 1665 (2015).

[36]T. N. Morgan, Phys. Rev. **148**, 890 (1966).

[37]M. Binder, B. Galler, M. Furitsch, J. Off, J. Wagner, R. Zeisel, and S. Katz, Appl. Phys. Lett. **103**, 221110 (2013).

[38]S. M. Sze and K. K. Ng, *Physics of Semiconductor Devices*, 3rd ed. (J. Wiley and Sons, Inc., New Jersey, USA, 2007).

[39]G. Baraf, Phys. Rev. B **55**, 10745 (1997).

[40]F. Römer and B. Witzigmann, Opt. Express **22**, A1440 (2014).

[41]S. Hafiz, F. Zhang, M. Monavarian, V. Avrutin, H. Morkoç, Ü. Özgür, S. Metzner, F. Bertram, J. Christen, and B. Gil, J. Appl. Phys. **117**, 013106 (2015).

[42]A. Laubsch, M. Sabathil, W. Bergbauer, M. Strassburg, H. Lugauer, M. Peter, S. Lutgen, N. Linder, K. Streubel, J. Hader, J. V. Moloney, B. Pasenow, and S. W. Koch, Phys. Status Solidi C **6**, S913 (2009).

[43]H.-S. Choi, D.-G. Zheng, H. Kim, and J.-I. Shim, J. Korean Phys. Soc. **66**, 1554 (2015).

[44]Y. C. Shen, G. O. Mueller, S. Watanabe, N. F. Gardner, A. Munkholm, and M. R. Krames, Appl. Phys. Lett. **91**, 141101 (2007).

[45]M. Zhang, P. Bhattacharya, J. Singh, and J. Hinckley, Appl. Phys. Lett. **95**, 201108 (2009).

[46]J. Iveland, L. Martinelli, J. Peretti, J. S. Speck, and C. Weisbuch, Phys. Rev. Lett. **110**, 177406 (2013).

[47]J. Hader, J. V. Moloney, and S. W. Koch, Appl. Phys. Lett. **96**, 221106 (2010).

[48]S. Hammersley, D. Watson-Parris, P. Dawson, M. J. Godfrey, T. J. Badcock, M. J. Kappers, C. McAleese, R. A. Oliver, and C. J. Humphreys, J. Appl. Phys. **111**, 083512 (2012).

[49]S. Okur, M. Nami, A. Rishinaramangalam, H. O. Sang, S. P. DenBaars, S. Liu, I. Brener, and D. F. Feezell, Opt. Express **25**, 2178 (2017).